Molecular MRI in the Earth's Magnetic Field using Continuous Hyperpolarization of a Biomolecule in Water

Philipp Rovedo[†], Stephan Knecht[†], Tim Bäumlisberger[†], Anna Lena Cremer[†], Simon B. Duckett[‡], Ryan E. Mewis[£], Gary G. R. Green[‡], Michael Burns[‡], Peter J. Rayner[‡], Dieter Leibfritz[†], Jan G. Korvink[$,€], Jürgen Hennig[†], Gerhard Pütz[§], Dominik von Elverfeldt[†] and Jan-Bernd Hövener[†,¥]*

†University Medical Center, Breisacher Str. 60 a, 79106 Freiburg, Germany

‡ Centre for Hyperpolarization in Magnetic Resonance, University of York, YO10 5DD, UK

£ School of Science and the Environment, Manchester Metropolitan University, Chester St., Manchester, M1 5GD, UK

$ Dept. of Microsystems Engineering, University Freiburg, Georges-Köhler-Allee 103, 79110 Freiburg, Germany

€ Freiburg Institute for Advanced Studies - FRIAS, Universität Freiburg, 79104 Freiburg

§Core Unit Clinical Chemistry, University Medical Center, Breisacher Str. 60 a, 79106 Freiburg

¥ German Consortium for Cancer Research (DKTK), Heidelberg, Germany

* jan.hoevener@uniklinik-freiburg.de, +49 761 270 93910

ABSTRACT

In this work, we illustrate a method to continuously hyperpolarize a biomolecule, nicotinamide, in water using *para*hydrogen and signal amplification by reversible exchange (SABRE). Building on the preparation procedure described recently by Truong *et al.* [*J. Phys. Chem. B*, 2014, 118,13882-13889], aqueous solutions of nicotinamide and an Ir-IMes catalyst were prepared for low-field NMR and MRI. The [1]H-polarization was continuously renewed and monitored by NMR experiments at 5.9 mT for more than 1000 s. The polarization achieved corresponds to that induced by a 46 T magnet (P = 1.6 · 10-4) or an enhancement of 10^4. The polarization persisted, although reduced, if cell culture medium (DPBS with Ca^{++} and Mg^{++}) or human cells (HL-60) were added, but was no longer observable after the addition of human blood. Using a portable MRI unit, fast [1]H-MRI was enabled by cycling the magnetic field between 5 mT and the Earth' field for hyperpolarization and imaging, respectively.

A model describing the underlying spin physics was developed that revealed a polarization pattern depending on both contact time and magnetic field. Furthermore, the model predicts an opposite phase of the dihydrogen and substrate signal after one exchange, which is likely to result in the cancelation of some signal at low field.

Introduction

The hyperpolarization (HP) of nuclear spins promises to overcome MRI's greatest impediment, its low sensitivity. In fact, ^{13}C-HP has been used successfully for metabolic MRI where it delivered significant insights into cancer metabolism *in vivo*.[1]

To date, however, most HP tracers in solution are hyperpolarized only once in an external polarizer. Typically, the hyperpolarization procedure is followed by a transfer of the sample to the imager, administration to the target organism and signal acquisition at 1.5 T or more. From the moment of its production, the HP decays exponentially with a characteristic time constant T_1 that rarely exceeds one minute and that depends on different factors including the magnetic field. During imaging, the transverse magnetization decays even faster with T_2, which is estimated of the order of 10^{-2} to 10^0 seconds.[2] Altogether, the hyperpolarization is inevitably lost over time by relaxation, readout and dilution.

Despite these challenges, the diagnostic potential of HP was impressively demonstrated in mice and men through the injection of a single bolus of hyperpolarized tracer.[1,3,4] Besides pyruvate, no other liquid tracer was injected into man yet.

Progress to prolong the relaxation of HP, however, is prospering with research into long-lived magnetization of elements like Lithium-6[5] or Silicon-29[6] and long-lived quantum states of multi-atomic systems[7,8] being particularly noteworthy.

Recently, a method to continuously hyperpolarize (cHYP) nuclear spins by means of *para*hydrogen (pH$_2$) and signal amplification by reversible exchange (SABRE, Scheme 1) was described.[9–13] The first reports of this effect at low field[10] demonstrated its potential and elucidated the underlying physical mechanism.[11] Its biological applicability, though, was limited because methanol and pyridine were used as solvent and substrate, respectively, both toxic. In

this contribution we seek to deliver low-field cHYP NMR and MRI of a biologically relevant agent in biologically relevant media.
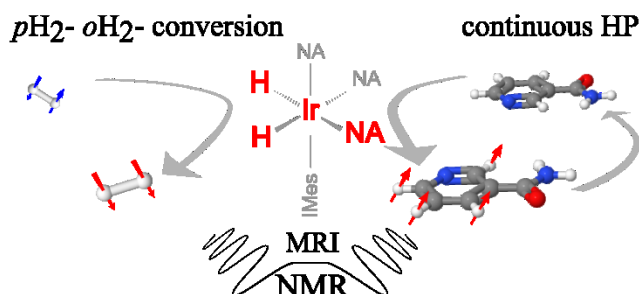
Scheme 1 | Continuous HP of nicotinamide (NA) using the spin order of pH_2 which is converted to oH_2 in the process. Note that non-magnetic pH_2 constitutes a pool of log-lived spin order that is impervious to depletion by MRI.

Methods

Chemistry

The method presented by Truong *et al.*[14] to obtain aqueous SABRE solutions was modified as described in the following. Either [IrCl(COD)(IMes)], [IMes = 1,3-bis(2,4,6-trimethylphenyl) imidazole-2-ylidene] (Ir-IMes)[15] or Crabtree's[16] catalyst was dissolved in deuterated methanol (MeOD, 99,8 % Carl Roth, Germany). To this solution, pyridine, pentafluorpyridine, nicotinamide (NA), adenine, adenosine or flavin adenine dinucleotide (FAD) were added. The latter molecules were chosen for their biological function. The catalyst was activated by exposing the solution to an elevated H_2 pressure of 10 bar for max. 20 min, yielding a transparent solution (Tab. 1). This solution was dried in an open beaker, and the residue was dissolved in either clinical 0.9 % NaCl solution, deionized H_2O or D_2O (99.8 %, Carl Roth, Germany). Cell

culture medium (DPBS (1X) with Ca++ and Mg++, Lonza Group Ltd, Switzerland), HL-60 cells and blood were added to the functional D_2O cHYP solution. Blood was added both wholly and in its components, cells and serum. No degassing was applied during the procedure.

The HL-60 cells were prepared on site ($\sim 4 \cdot 10^6$ cells in RPMI 1640 with L-glutamine, without glucose, Lonza Group Ltd, Switzerland). The cell medium in which the HL-60 cells were suspended, among other salts, contained $NaHCO_3$ (24 mM), L-Glutamine (2 mM), KCl (5 mM) and NaCl (103 mM). Prior to the HP experiments, the cells were separated from the medium by centrifugation (5 min, 800 G, Eppendorf 5702RH, Germany) and dissolved in 1 ml D_2O. Fresh, whole human blood was used with or without coagulant (NH_4, EDTA, S-Monovette 2.7 / 9 ml, Sarstedt, Germany). Blood plasma or blood cells were obtained by centrifuging fresh blood for 5 min at 800 G.

Both 4,6-$^2H_2$ nicotinamide and Ir-IMes catalyst were synthesized as described before (U. York).[15] All other chemicals were purchased and used without further purification.

| No.	Catalyst (mg)		Substrate		Solvent (ml)	
1	Ir-IMes	4	Pyridine	12 μl	D_2O	5
2	Ir-IMes	4	Nicotinamide	40 mg	D_2O	5
3	Ir-IMes	4	Pyridine	15 μl	D_2O + DPBS	5 + 1
4	Ir-IMes	4	Pyridine	15 μl	D_2O + HL60 cells	5 + 1
5	Ir-IMes	4	Nicotinamide	40 mg	D_2O + whole blood, cells, serum	5 + 1
6	Ir-IMes	4	FAD	87 mg	D_2O	5
7	Ir-IMes	4	Adenosine	26 mg	D_2O	10
8	Ir-IMes	4	Adenine	13 mg	D_2O	5
9	Ir-IMes	4	Pentafluor-pyridine	16 μl	D_2O	5
10	Crabtree	6	Adenine	10 mg	10	10
11	Crabtree	6	Pentafluor-pyridine	24 μl	10	10

Table 1 | Catalysts, substrates and solvents used for cHYP experiments. All listed combinations were exposed to pH$_2$ within the low field NMR setup. cHYP was observed for combinations No. 1-4 (green). Volatile substrates such as pyridine were added to the final, activated D$_2$O solution.

High-field NMR

High-field ^{1}H NMR spectra were acquired at 600 MHz (Bruker, USA). pH$_2$ was bubbled into the sample through a capillary at 5.9 mT for 10 s before the sample was transferred to the spectrometer within ~ 5 - 10 s. The spectrum was recorded after one 90 ° excitation with an acquisition delay of 0.04 s. The concentrations were comparable to those used in the low field experiments (12 mg nicotinamide and 1 mg IrIMes in 1 ml D$_2$O).

Low-field NMR

Low-field ^{1}H-NMR spectra were acquired with a modified low-field unit described by Borowiak *et al* [19] (Figure 1). These experiments were *in situ* with respect to B_0 and sample position.
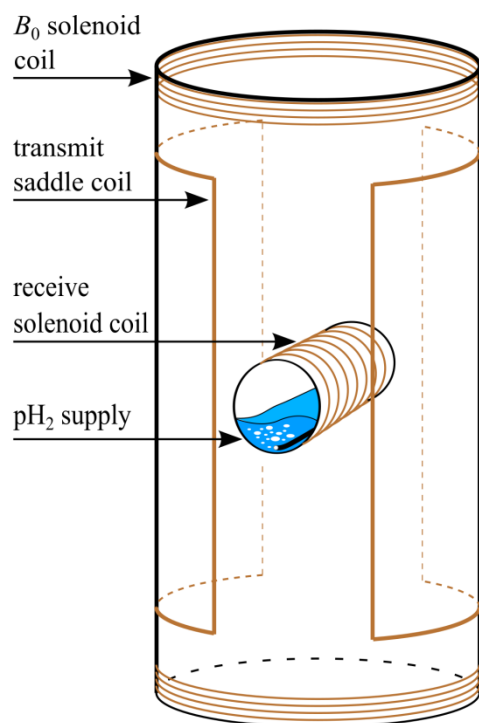
Figure 1 | Schematic view of the low-field NMR spectrometer used for cHYP, including coils for the static field B_0, the excitation pulses and for signal detection. Inside the detection coil, pH$_2$ was bubbled through the solution containing substrate and catalyst.

Signal generation and reception were realized with commercial hardware (DAC USB 6251, National Instruments, USA), controlled by custom software (MATLAB, The Mathworks, USA). Excitation pulses were applied *via* an audio amplifier (TX-8555, Onkyo, Japan, gain 63) using a saddle-shaped, untuned and unmatched excitation coil.[20,21] The receive circuit was a custom built solenoid coil wound around a syringe (28 mm x 65 mm, $\approx$ 500 windings of 0.3 mm copper wire in two layers, tuned to $\approx$ 250 kHz, no matching). All three coils were aligned on perpendicular axes. To calibrate the flip angles, the syringe was filled with 29 ml water doped with a Gadolinium-based relaxation agent 1:100 (Magnetvist, Bayer-Schering). All data were acquired with 90° excitation pulses with a length of 700 μs and an amplitude of 2.55 V or 39 V at the

output of the digital-to-analog converter or across the transmit coil, respectively. A total of 100.000 points (including the excitation pulse) was acquired at a sampling rate of 1 MHz with a 16 bit resolution of an input voltage range of $\pm$ 0.1 V. The first 2000 to 2400 points (2 ms – 2.4 ms) were discarded before the Fourier transformation to avoid signal originating from the excitation pulse. The syringe comprised an inlet and outlet for pH$_2$, which was supplied continuously during the HP measurements at atmospheric pressure.

Signal quantification

The signal was quantified using the area of a Lorentzian function fitted to the Fourier-transformed data, which was zero-filled once and multiplied by an exponential decay function with a time constant of 5 ms which is of the order of T$_2{}^*$. Errors on the fitted areas were estimated *via* the product of the standard deviation of the noise and twice the line width. The noise was measured at 95 % of the frequency of the peak.

The polarization yield (P) per molecule was determined by comparing the HP signal to the signal obtained from a 29 ml water sample acquired using identical acquisition parameters but in thermal equilibrium at 5.9 mT.

The re-hyperpolarization of a given sample was monitored by consecutive, 90°-acquisitions with a varying repetition time (TR) between 1 s and 30 s. A saturation recovery function was fitted to the average signal from each TR series [A(TR) = a exp(-b·TR) + c]. The first data point of each series was omitted.

For low-field NMR, the SNR was calculated by dividing the fitted signal height by the standard deviation of the noise (Matlab). For Earth-field MRI, the SNR was calculated by dividing the mean signal of a region of interest (ROI) within the samples by the standard

deviation of the noise in a ROI void of signal using a scientific image processing software (ImageJ).[22]

Low-field MRI

Two cylindrical tubes (100 mm length, 24 mm diameter) were filled with 20 ml H_2O or 70 mM nicotinamide, 1.3 mM catalyst in 5 ml D_2O and placed in a commercial Earth-field MRI (Magritek Terranova, NZ).

2D projection spin-echo images were acquired by applying a magnetic field of ≈ 5.9 mT for 5 s for hyperpolarization, followed by spatial encoding, signal excitation and data acquisition in the shimmed Earth's magnetic field. One phase encoding step was executed per excitation, resulting in a scan time of 5:20 min for a 32·32 matrix, field of view of $(100 \text{ mm})^2$ with a repetition time of 10 s and an echo time of 150 ms. The apparent voxel size was decreased to $(1.6 \text{ mm})^2$ by zero filling once. Flip angles were calibrated on a 20 ml water phantom. We refer to these experiments as *in situ* with respect to the positioning of the sample, but not with respect to the magnetic field which was cycled.

Parahydrogen

pH_2 was enriched from H_2 (99.999 % purity) using the setup described by Hövener *et al.* [23] at 21 K. The pH_2 fraction was quantified by MR to 95 ± 5 %. pH_2 was stored in 1.7 l aluminum gas bottles at room temperature and 35 bar.

Simulations

Using established theory[24,25] and a density-matrix based frame work that was described before[8], cHYP (*in-situ* SABRE) was simulated in a model that now includes all of the protons with a relevant coupling to H_2 (spins 2, 4-6, Fig. 3). The model describes a situation where the H_2-NA complex is formed *ad hoc* at $t = 0$ s for a duration t_c. We assume that H_2 is in the para-state and that NA is non-polarized at $t = 0$. In the following period t_c, H_2 and NA entertain a J-coupling network that enables transfer of spin order. After t_c, coherences are eliminated as they are bound to average out during the following, free evolution period.

To investigate the effect of overlapping resonances of H_2 and NA at low field, their different T_1 relaxation constants were considered in the simulations.

J-coupling constants of the substrate were calculated (using a software provided by EPFL, http://www.nmrdb.org/),[26] substrate-hydride couplings were extracted from Adams and coworkers.[27] The values for *para*hydrogen ($pH_{2,i}$) and NA (NA_j) are listed in Tab. 2.

Chemical shifts (ppm)					
$pH_{2,1}$	$pH_{2,2}$	NA_2	NA_4	NA_5	NA_6
-22	-22	8.89	8.04	7.55	8.55
J-couplings (Hz)					
	$pH_{2,2}$	NA_2	NA_4	NA_5	NA_6
$pH_{2,1}$	7	0.1	0	0	3
$pH_{2,2}$		0	0	0	0.1
NA_2			1.2	4.5	1.9
NA_4				8	1.9
NA_5					4.6

Table 2 | Chemical shifts and J-couplings for pH_2 and NA used in the simulations.

Results and Discussion   At the low magnetic field used here and with a line width of the order of 10 - 100 Hz, no chemical shifts were resolved in the experiments and the assignment of the signal to individual molecules was not feasible. The simulations, however, allowed us to shed more light on the underlying physics of the effect.

In the simulations, it was found that, after one exchange, all spins of the hyperpolarized substrate carry the same phase, i.e. that their signals are expected to add-up positively.

Furthermore, we found that the summed polarization of NA remains the same if the positions without a J-coupling to pH_2 were deuterated (NA-4,5), as expected.

In contrast, the polarization was dramatically reduced if the nucleus NA-6, that has the strongest coupling to $pH2$, was deuterated.

This finding may be supported by qualitative experiments at low field where the ^{1}H-signal from nicotinamide-D_2 isomer (4 and 6 positions deuterated) was reduced approx. two fold compared to protio-nicotinamide (not shown). This observation may be explained by the partial loss of the proton with the strongest J-coupling to pH_2, depending on the binding orientation of the substrate to Ir.

In a previous report,[28] it was shown that 3,4,5-^{2}H$_3$-pyridine, which is deuterated at the positions distant to pH_2, provided more MRI signal than protio-pyridine. While the simulations here suggest that the total signal of both molecules should be the same, the discrepancy may be attributed to a prolonged ^{1}H relaxation time of 3,4,5-^{2}H$_3$-pyridine, which is neglected in our calculations.

Furthermore, the simulations indicated that the H_2 (as hydride or in solution) is hyperpolarized as well, e.g. as observed by Barskiy.[29] The H_2 signal exhibited the same magnitude as, but opposite phase than the summed NA signal (disregarding relaxation). As a consequence, at low field, the signals cancel out if the peaks collapse. The fact that strong net signal was observed experimentally by us and others[30] may be attributed to different relaxation rates of H_2 and NA. This hypothesis is supported by the finding that the cancelation was attenuated when relaxation with different constants for NA and H_2 was added to the simulations.

The extent of the predicted signal cancelation was dependent on the ratio of the NA and H_2 relaxation time constants. We assumed that H_2 and hydride relax faster than the substrate $T_1(substrate) > T_1(H_2)$, which is supported by the high field spectrum (Fig. 2), where H_2 and substrate signal have opposite phase, the H_2 signal was not visible and the hydride signal is smaller than the substrate signals.

A similar observation was made in other work,[29] where a similar phase pattern was found. Here, the hyperpolarized H_2 signal was significantly larger when the data was acquired instantaneous during high-field SABRE HP (with little relaxation delay) as compared to low-field HP and transfer to high field, where a few seconds delay occurred.

The signal cancelation may significantly reduce the observed signal. This effect may be elucidated by a more homogeneous field that allows the distinction of hydride (-22 ppm) and substrate (8 − 9 ppm). Perdeuterated substrate may help to resolve this question; perfluorinated pyridine did not yield observable cHYP.
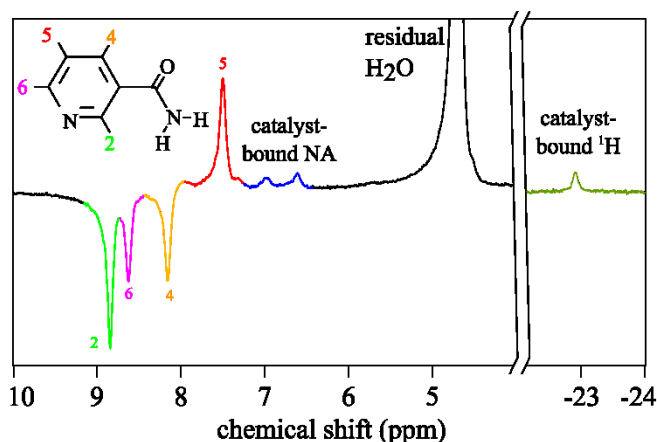
Figure 2 | ^{1}H-NMR spectrum of SABRE-HP NA and hydride in D_2O, acquired at 600 MHz. The sample was exposed to pH_2 in a resistive magnet at 5.9 mT for ~30 s, and transferred to the NMR in ~ 5 - 10 s where the data was recorded after a 90° excitation. During the transfer, the sample was exposed to the Earth's field and the stray field of the spectrometer, which may account for the distinct phase pattern of NA. Note that the signals of NA are much larger than the hydride, and that no signal of H_2 in solution was observed.

Furthermore, we found a distinct polarization transfer pattern that depends both on contact time t_c and the magnetic field B_0 (Fig. 3), similar to the dependency for pyridine that was observed experimentally before.[11] This result helps to identify the optimal contact time t_c, which is sensitive to different ligands of the catalyst or the reaction temperature.[15,31]

The simulated, summed signal of all substrate spins reached a maximum at a field $B_0 = 5.3$ mT and a contact time $t_c = 300$ ms. Using these parameters, the average polarization level for each NA spin was simulated to P = 20 %. This value was obtained by summing the polarizations of all spins $NA_{2, 4-6}$, divided by the number of spins (four). The polarization of the $NA_{2, 6}$ spins was in the same order of magnitude as that of $NA_{4, 5}$ despite the fact that no direct coupling between

pH$_2$ and NA$_{4,5}$ was considered, i.e. the polarization is efficiently spread among the strongly coupled substrate nuclei.

The inclusion of all contributing nuclei did not fundamentally change the polarization transfer pattern as function of B_0 and t_c.

It should be noted that the simulations assume that all molecules make contact with the pH$_2$ only once, at the same time and for the same duration. This is a simplification of the real situation where only a fraction of the molecules is polarized at a given time and multiple chemical exchanges occur. Such considerations of chemical kinetics are treated elsewhere[32] and are beyond the scope of the qualitative analysis provided here.
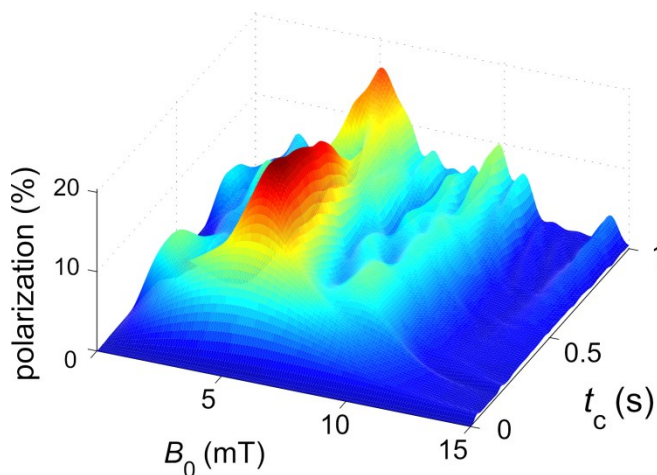
Figure 3: Simulated cHYP of nicotinamide after interaction with pH$_2$ as a function of magnetic field B_0 and contact time t_c. A maximum mean polarization of P = 20 % was found at B_0 = 5.3 mT and t_c = 300 ms. Note that the average polarization of all contributing nicotinamide hydrogens is shown and that a contribution from H$_2$ is neglected.

Continuous Hyperpolarization of NA in water

As expected, a sample of 70 mM NA in D_2O did not yield observable ^{1}H-MR signal when 200 thermal 90° acquisitions at 5.6 mT were summed up. This is because the population difference across the magnetic states at 5.6 mT is so small that even a 30 ml H_2O sample yielded a SNR of 7.75 only, under otherwise identical acquisition parameters.

While supplying pH$_2$, a strongly hyperpolarized ^{1}H-NMR signal with a SNR = 56 was detected and maintained for more than 1000 s. Neglecting the contribution of H_2 and hydride to the signal, this signal corresponds to a polarization of $P = 1.6 \cdot 10^{-4}$, i.e. a signal enhancement of 9300.

While we were not able to elucidate the composition of the signal at low field, both simulations and high-field NMR spectra indicate that the contribution of H_2 or hydride will be detrimental and reduce the overall signal. As a consequence, it is likely that the "apparent" polarization reported above is underestimated.

The polarization level may appear low with respect to bolus ^{13}C-HP and cHYP in methanol, where $P \approx 10^{-1}$ and $P \approx 10^{-3}$, respectively, were reported. However, the enhancement is available continuously for more than 1000 s until adequate SNR is obtained by repetitive acquisitions.

By variation of the repetition time (TR) between excitations, the re-polarization process was monitored and a mono-exponential polarization recovery with a time constant of $T_{pr} = 5.4 \pm 0.2$ s was found (NA in D_2O at 5.9 mT, 1.3 mM Ir-IMes, 70 mM NA, Fig. 4).

This repolarization time is similar to the T_1 recovery of ^{1}H signal *in vivo* and substantially hyperpolarized signal was re-gained already after two seconds.

For clinical MRI and high-resolution NMR, the T_1 recovery is essential because it enables repetitive signal excitation and signal averaging. For conventional hyperpolarization, however,

the concept of signal averaging is limited. cHYP, in contrast, allows *in-situ* re-hyperpolarization

for an extended period of time. Given the sample used in Fig. 4, e.g., 30 scans acquired in one

minute would yield an SNR of $\sqrt{\frac{t_{aq}}{TR}} \cdot \cos(\alpha_E) \cdot SNR = \sqrt{60s\,/\,2\,s} \cdot 0.72 \cdot 56 = 220$ using

the Ernst angle of $\alpha_e = \arcos(\exp(-TR/T_{pr})) = 46\,°$ and assuming a linear dependence of SNR and

$\cos(\alpha)$.

The gain in SNR may be used to lower the limit of detection, although some restrictions apply

for low substrate concentrations as described in.[33]

To obtain a thermal polarization equal to the one observed in our 5-mT experiments, a

magnetic field of ≈ 46 T is required. We expect to improve the SNR further by using more

advanced experimental equipment, in particular more sensitive detection hardware and

sequences.
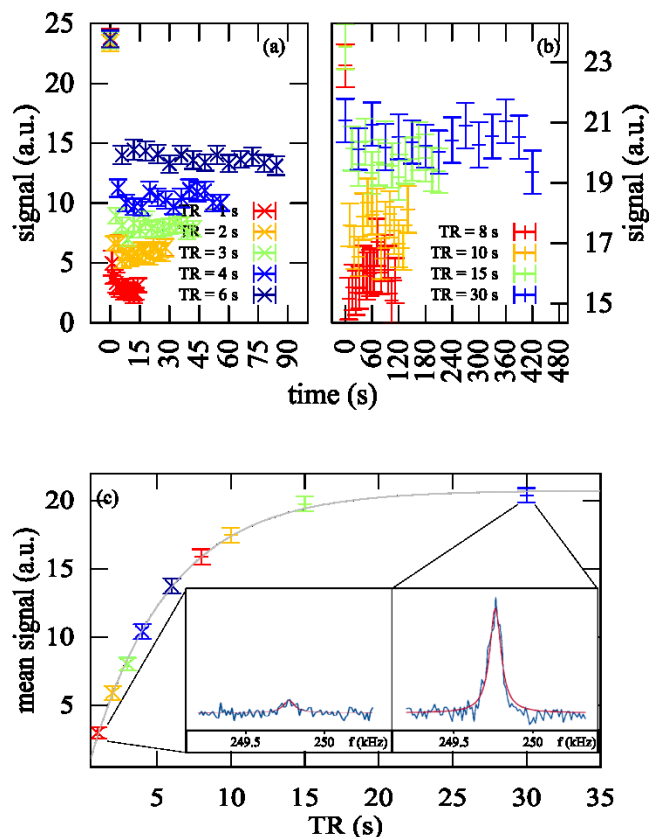
Figure 4 │ Re-hyperpolarization of 70 mM nicotinamide. A cascade of 90° pulses with variable repetition time (TR) was used to monitor the re-hyperpolarization process *in situ* at 5.9 mT (a, b), where each data point corresponds to the signal of one 90° acquisition. One solution was used to acquire all data, corresponding to cHYP for more than 1000 s. A saturation recovery function that was fitted to the mean signal of each TR series (c) yielded a repolarization time constant of $T_{pr} = (5.4 \pm 0.2)$ s. In H_2O, a similar experiment yielded a time constant of $T_{pr} = (2.4 \pm 0.4)$ s. Representative spectra and fits are shown in the insets. Catalyst concentration was 1.3 mM, NA and Ir-IMes were dissolved in 5 ml D_2O

Continuous Hyperpolarization of other substrates and media

The cHYP signal persisted, although reduced, when cell culture medium or HL-60 cells (Fig. 5) were added to Ir-IMes with NA or pyridine in D_2O, respectively. Note that this is a first proof of concept only, and it is known that cHYP is reduced in biofluids.[10] Of course, cells are not viable in D_2O, but within the short observation time, cells should remain intact. On the other hand, the observation time frame of 90 s readily allows interaction of pyridine with the cell membranes; deprotonated pyridine may even enter the cells by diffusion. A more thorough investigation especially towards the viability of the cells will follow. Unfortunately, our attempts to cHYP other relevant biomolecules were unsuccessful (Tab. 1). Reasons may include inefficient exchange reactions and J-couplings as well as relaxation.

Still, it is promising that cHYP with Ir-IMes catalyst remained functional in cell-culture medium and when cells were added. When blood was added, however, the signal dropped below the limit of detection. In previous experiments, the cHYP signal of pyridine in MeOD was reduced but pertained after blood was added.[10] Denaturation and subsequently precipitation of blood components like proteins and salts may be more pronounced in MeOD than in D_2O. Note, though, that in this experiment the polarization was 10 times higher than for NA in D_2O as reported here. We speculate that blood components suppress the exchange of substrate and hydrogen at the catalyst and that faster relaxation occurs.
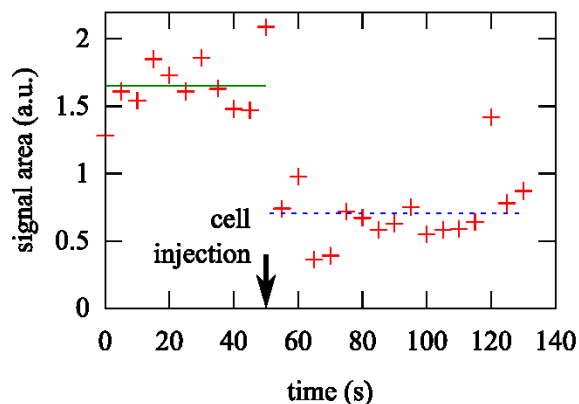
Figure 5: Signal of continuously hyperpolarized pyridine (37 mM) in D$_2$O (5 ml) before and after HL-60 cells (~ 4·10^6) were added. Each data point represents the fitted area of the observed resonance, acquired after 90°-excitations interleaved by a 5 s delay. The cells were added after scan No. 11 (50 s, indicated by an arrow), and the mean signals before and after the injection are indicated by a solid green and dashed blue line. Note that cHYP was reduced but remained functional.

Earth-field MRI of continuously hyperpolarized NA in water

Within five minutes, cHYP MRI of NA in D$_2$O was acquired with a SNR of 13.5 (Figure 6). The water sample yielded a SNR of 4.7 only, despite the fact that the concentration of water was 785 times higher than that of NA, corresponding to ≈ 3300 more molecules and 3300 / 2 more (contributing) protons.

This corresponds to an overall enhancement of 4740 for each NA proton (SNR$_{HP}$ / SNR$_{H2O}$) · (amount of protons in H$_2$O / amount of contributing protons in NA).

Note that the imaging experiment was relatively long because of the time-consuming cycling between the field for cHYP B_{pol} ≈ 5.9 mT and Earth' field B_0 ≈ 52 µT for signal acquisition;

this step was necessary for every k-space line. If the signal were to be acquired without cycling but directly at 5.9 mT, we estimate that no more than one minute would be required to yield an image with the same resolution and a SNR of 10 (assuming a spin echo sequence, Ernst angle of $\alpha_e = 46°$ and one k-space line per spin echo).

The concept of *in-situ* SABRE MRI was demonstrated by Barskiy *et al.*,[30] although at an elevated field of 47.5 mT, where it is likely that a less efficient, non-coherent transfer mechanism responsible for the hyperpolarized signal. The acquisition of multiple k-space lines,[34] multiple spin echoes or multiple slices is expected to further accelerate the imaging or lower the limit of detection correspondingly.
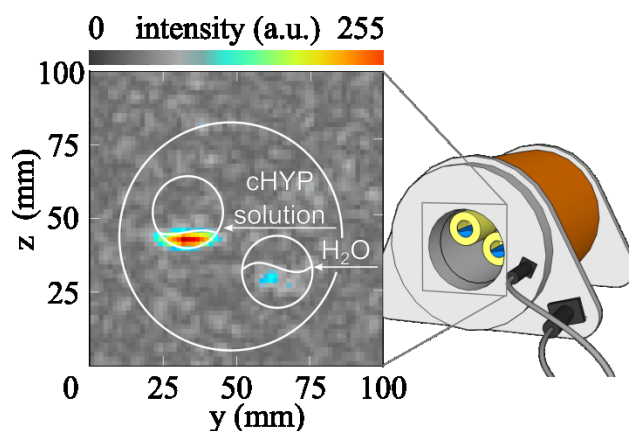
Figure 6 │ Molecular MRI of nicotinamide in the Earth's magnetic field enabled by cHYP with an image resolution of (1.6 mm)^2, acquired in 5:20 min (left). Continuously hyperpolarized NA (70 mM) in 5 ml D_2O yielded a SNR of 13.4, considerably stronger than the signal of water (55 M) with a SNR of 4.7. Before the data was acquired in the Earth' field, cHYP of NA and prepolarization of H_2O were carried out for 5 s at 5.9 mT. Catalyst concentration was 1.3 mM, white lines indicate approximate position of samples and solutions. For better visualization, the noise level was set to grayscale.

Low-field MRI of a biomolecule in water is an important milestone towards a possible *in-vivo* application for continuously hyperpolarization by SABRE. At the current stage, this technique is still in its infancy. Still, it is worthwhile to make some estimations on the general feasibility of this goal. It is instructive to consider the following factors: (i) the limit of sensitivity, (ii) the functionality and toxicity of cHYP *in vivo* and (iii) the question if sufficient pH_2 is transported to the relevant structures at all.

(i) The sensitivity of cHYP MRI depends on the magnetization and how efficiently it is detected. The detection efficiency will be improved by real *in-situ* acquisition, more sophisticated sequences, a more homogeneous B_0 field, preamplifiers for signal detection or coils with higher quality factor or even cooled to cryogenic temperature.[35] Altogether, an improvement in sensitivity by a factor of 10 or more appears feasible.

The observable magnetization will be improved by a higher polarization yield and less signal cancelation. The former may be achieved by the optimization of the cHYP catalyst and substrate and its parameters such as pressure, temperature and concentrations, as far as these are accessible. Besides optimal parameters for the polarization transfer, the exchange kinetics and relaxation time play an important role when it comes to overall signal. The latter may be improved by employing X-nuclei whose SABRE hyperpolarization was already reported.[28,36–38] An additional advantage of using X-nuclei would be the reduction of background signal.

(ii) In fact, the current chemical system (Ir-IMes and NA) may, to some extent, already be functional in blood, but the sensitivity may be too low to detect it. Earlier results have shown that a reduced cHYP persists if blood was added to pyridine and Ir-IMes in MeOD.[10] The current

complex however was not designed with an *in-vivo* application in mind, and even a catalyst of limited biocompatibility may still be valuable for preclinical application. To the knowledge of the authors, no dedicated toxicity study was performed yet. Note that no degradation of catalyst efficiency was observed during the timescales reported here.

(iii) It is instructive to elaborate on how much polarization is required for imaging, and how this compares to the current experiments and the amount of $p\mathrm{H}_2$ available.

In current state-of-the-art, routine whole-body MRI scanner, images with a voxel size of $(600\ \mu\mathrm{m})^3$ were acquired at 3T using a head coil and a RARE[39] sequence in five minutes acquisition time[40] or $(350\ \mathrm{mm})^3$ using a specialized coil in conjunction with a gradient echo sequence.[41,42] Given a $^1\mathrm{H}$ polarization of $3\cdot10^{-6}$ per Tesla and a concentration of 80 M of $^1\mathrm{H}$ *in vivo*, this corresponds to an concentration of approximately 720 µM or an amount of substance of approximately $150\cdot10^{-12}$ mol of completely polarized (P = 100 %) spins per voxel (one fifth of that for the second example).

The H_2 concentration *in-vivo* (after inhalation or other H_2-exposure) was measured to be in the range of 1 µM to 1 mM,[43] and may be elevated by using a hyperbaric H_2 atmosphere as demonstrated in a remarkable experiment before.[44]

Sufficient signal for MRI would for example be obtained if 40 µM $p\mathrm{H}_2$ was to be converted to polarization with approx. 1 % efficiency (Tab. 3). Thus, it appears that a sufficiently high concentration of $p\mathrm{H}_2$ *in vivo* is attainable *in vivo*, given that an efficient transfer mechanism is available. For this transfer mechanism, the catalyst will play a key role.

Note that the consumption and renewal of $p\mathrm{H}_2$ wasn't taken into account in this estimation, and neither was the effect of the resonance frequency, although this effect may be neglected under certain conditions.[45] The required polarization per voxel was estimated for a standard, whole-

body MRI system, and may be reduced significantly by using e.g. a cryogenic coil or SQUID for signal reception.[46]

Voxel volume	Assumed pH_2 concentration	Required efficiency
$(2\ mm)^3$	20 μM	92 %
$(5\ mm)^3$	20 μM	6 %
$(10\ mm)^3$	20 μM	0.75 %

Table 3 | Transfer efficiency of pH_2-spin order into observable polarization that is required to obtain $150 \cdot 10^{-12}$ mol of completely polarized spins per voxel at a given pH_2 concentration. This amount of polarized spins was used to acquire high-resolution MRI *in vivo*.[40]

Altogether, the prospect of continuously re-hyperpolarizing molecules is intriguing and would be a major advancement for biomedical imaging. It promises a breakthrough in specificity for molecular imaging as well as applicability of MRI e.g. for portable devices. An alternative approach to depict processes that are below the limit of detection is chemical exchange saturation transfer (CEST),[47] where the accumulated effect of a relatively small amount of substance (that is not directly detectable) on the abundant water protons is used, or hyperCEST, where HP Xenon is depleted in targeted biosensors.[48] Overhauser dynamic nuclear polarization was used to enhance the signal of water for low field MRI, although a radical is required for this technique.[49] pH_2-based cHYP is the latest addition to these techniques and appears to be a promising approach towards the goal of *in vivo* hyperpolarization, despite the fact that some hurdles persist and that no *in vivo* application was shown yet.

AUTHOR INFORMATION

Notes

The authors declare no competing financial interests.

References

(1) Nelson, S. J.; Kurhanewicz, J.; Vigneron, D. B.; Larson, P. E. Z.; Harzstark, A. L.; Ferrone, M.; Criekinge, M. van; Chang, J. W.; Bok, R.; Park, I.; et al. Metabolic Imaging of Patients with Prostate Cancer Using Hyperpolarized [1-13C]Pyruvate. *Sci. Transl. Med.* **2013**, *5* (198), 198ra108.

(2) Leupold, J.; Månsson, S.; Petersson, J. S.; Hennig, J.; Wieben, O. Fast Multiecho Balanced SSFP Metabolite Mapping of 1H and Hyperpolarized 13C Compounds. *Magn. Reson. Mater. Phys. Biol. Med.* **2009**, *22* (4), 251–256.

(3) Day, S. E.; Kettunen, M. I.; Gallagher, F. A.; Hu, D.-E.; Lerche, M.; Wolber, J.; Golman, K.; Ardenkjaer-Larsen, J. H.; Brindle, K. M. Detecting Tumor Response to Treatment Using Hyperpolarized 13C Magnetic Resonance Imaging and Spectroscopy. *Nat. Med.* **2007**, *13* (11), 1382–1387.

(4) Gallagher, F. A.; Kettunen, M. I.; Day, S. E.; Hu, D.-E.; Ardenkjær-Larsen, J. H.; Zandt, R. in 't; Jensen, P. R.; Karlsson, M.; Golman, K.; Lerche, M. H.; et al. Magnetic Resonance Imaging of pH in Vivo Using Hyperpolarized 13C-Labelled Bicarbonate. *Nature* **2008**, *453* (7197), 940–943.

(5)   van Heeswijk, R. B.; Uffmann, K.; Comment, A.; Kurdzesau, F.; Perazzolo, C.; Cudalbu, C.; Jannin, S.; Konter, J. A.; Hautle, P.; van den Brandt, B.; et al. Hyperpolarized Lithium-6 as a Sensor of Nanomolar Contrast Agents. *Magn. Reson. Med.* **2009**, *61* (6), 1489–1493.

(6)   Cassidy, M. C.; Chan, H. R.; Ross, B. D.; Bhattacharya, P. K.; Marcus, C. M. In Vivo Magnetic Resonance Imaging of Hyperpolarized Silicon Particles. *Nat. Nanotechnol.* **2013**, *8* (5), 363–368.

(7)   Pileio, G.; Carravetta, M.; Levitt, M. H. Storage of Nuclear Magnetization as Long-Lived Singlet Order in Low Magnetic Field. *Proc. Natl. Acad. Sci.* **2010**, *107* (40), 17135–17139.

(8)   Feng, Y.; Davis, R. M.; Warren, W. S. Accessing Long-Lived Nuclear Singlet States between Chemically Equivalent Spins without Breaking Symmetry. *Nat. Phys.* **2012**, *8* (11), 831–837.

(9)   Adams, R. W.; Aguilar, J. A.; Atkinson, K. D.; Cowley, M. J.; Elliott, P. I. P.; Duckett, S. B.; Green, G. G. R.; Khazal, I. G.; López-Serrano, J.; Williamson, D. C. Reversible Interactions with Para-Hydrogen Enhance NMR Sensitivity by Polarization Transfer. *Science* **2009**, *323* (5922), 1708–1711.

(10) Hövener, J.-B.; Schwaderlapp, N.; Lickert, T.; Duckett, S. B.; Mewis, R. E.; Highton, L. A. R.; Kenny, S. M.; Green, G. G. R.; Leibfritz, D.; Korvink, J. G.; et al. A Hyperpolarized Equilibrium for Magnetic Resonance. *Nat. Commun.* **2013**, *4* (2946).

(11) Hövener, J.-B.; Knecht, S.; Schwaderlapp, N.; Hennig, J.; von Elverfeldt, D. Continuous Re-Hyperpolarization of Nuclear Spins Using Parahydrogen: Theory and Experiment. *ChemPhysChem* **2014**, *15* (12), 2451–2457.

(12) Pravdivtsev, A. N.; Yurkovskaya, A. V.; Vieth, H.-M.; Ivanov, K. L. RF-SABRE: A Way to Continuous Spin Hyperpolarization at High Magnetic Fields. *J. Phys. Chem. B* **2015**.

(13) Eshuis, N.; Aspers, R. L. E. G.; van Weerdenburg, B. J. A.; Feiters, M. C.; Rutjes, F. P. J. T.; Wijmenga, S. S.; Tessari, M. 2D NMR Trace Analysis by Continuous Hyperpolarization at High Magnetic Field. *Angew. Chem. Int. Ed.* **2015**.

(14) Truong, M. L.; Shi, F.; He, P.; Yuan, B.; Plunkett, K. N.; Coffey, A. M.; Shchepin, R. V.; Barskiy, D. A.; Kovtunov, K. V.; Koptyug, I. V.; et al. Irreversible Catalyst Activation Enables Hyperpolarization and Water Solubility for NMR Signal Amplification by Reversible Exchange. *J. Phys. Chem. B* **2014**.

(15) Cowley, M.; Adams, R.; Atkinson, K.; Cockett, M.; Duckett, S.; Green, G.; Lohmann, J. A. B.; Kerssebaum, D. K.; Mewis, R. E. Iridium N-Heterocyclic Carbene Complexes as Efficient Catalysts for Magnetization Transfer from Para-Hydrogen. *J. Am. Chem. Soc.* **2011**, *133*, 6134–6137.

(16) Crabtree, R. H.; Lavin, M.; Bonneviot, L. Some Molecular Hydrogen Complexes of Iridium. *J. Am. Chem. Soc.* **1986**, *108* (14), 4032–4037.

(17) Chou, C.-Y.; Ferrage, F.; Aubert, G.; Sakellariou, D. Simple Method for the Generation of Multiple Homogeneous Field Volumes inside the Bore of Superconducting Magnets. *Sci. Rep.* **2015**, *5*.

(18) Ivanov, K. L.; Pravdivtsev, A. N.; Yurkovskaya, A. V.; Vieth, H.-M.; Kaptein, R. The Role of Level Anti-Crossings in Nuclear Spin Hyperpolarization. *Prog. Nucl. Magn. Reson. Spectrosc.* **2014**, *81*, 1–36.

(19) Borowiak, R.; Schwaderlapp, N.; Huethe, F.; Lickert, T.; Fischer, E.; Bär, S.; Hennig, J.; Elverfeldt, D.; Hövener, J.-B. A Battery-Driven, Low-Field NMR Unit for Thermally and Hyperpolarized Samples. *Magn. Reson. Mater. Phys. Biol. Med.* **2013**, *26* (5), 491–499.

(20) Hövener, J.-B.; Chekmenev, E.; Harris, K.; Perman, W.; Robertson, L.; Ross, B.; Bhattacharya, P. PASADENA Hyperpolarization of 13C Biomolecules: Equipment Design and Installation. *Magn. Reson. Mater. Phys. Biol. Med.* **2009**, *22* (2), 111–121.

(21) Hövener, J.-B.; Chekmenev, E. Y.; Harris, K. C.; Perman, W. H.; Tran, T. T.; Ross, B. D.; Bhattacharya, P. Quality Assurance of PASADENA Hyperpolarization for 13C Biomolecules. *Magn. Reson. Mater. Biol. Phys. Med.* **2009**, *22* (2), 123–134.

(22) Schneider, C. A.; Rasband, W. S.; Eliceiri, K. W. NIH Image to ImageJ: 25 Years of Image Analysis. *Nat. Methods* **2012**, *9* (7), 671–675.

(23) Hövener, J.-B.; Bär, S.; Leupold, J.; Jenne, K.; Leibfritz, D.; Hennig, J.; Duckett, S. B.; von Elverfeldt, D. A Continuous-Flow, High-Throughput, High-Pressure Parahydrogen Converter for Hyperpolarization in a Clinical Setting. *NMR Biomed.* **2012**, DOI: 10.1002/nbm.2873.

(24) Pravdivtsev, A. N.; Ivanov, K. L.; Yurkovskaya, A. V.; Petrov, P. A.; Limbach, H.-H.; Kaptein, R.; Vieth, H.-M. Spin Polarization Transfer Mechanisms of SABRE: A Magnetic Field Dependent Study. *J. Magn. Reson. San Diego Calif 1997* **2015**, *261*, 73–82.

(25) Adams, R. W.; Duckett, S. B.; Green, R. A.; Williamson, D. C.; Green, G. G. R. A Theoretical Basis for Spontaneous Polarization Transfer in Non-Hydrogenative Parahydrogen-Induced Polarization. *J. Chem. Phys.* **2009**, *131* (19), 194505.

(26) Binev, Y.; Marques, M. M. B.; Aires-de-Sousa, J. Prediction of 1H NMR Coupling Constants with Associative Neural Networks Trained for Chemical Shifts. *J. Chem. Inf. Model.* **2007**, *47* (6), 2089–2097.

(27) Adams, R. W.; Duckett, S. B.; Green, R. A.; Williamson, D. C.; Green, G. G. R. A Theoretical Basis for Spontaneous Polarization Transfer in Non-Hydrogenative Parahydrogen-Induced Polarization. *J. Chem. Phys.* **2009**, *131* (19), 194505.

(28) Hövener, J.-B.; Schwaderlapp, N.; Borowiak, R.; Lickert, T.; Duckett, S. B.; Mewis, R. E.; Adams, R. W.; Burns, M. J.; Highton, L. A. R.; Green, G. G. R.; et al. Toward Biocompatible Nuclear Hyperpolarization Using Signal Amplification by Reversible Exchange: Quantitative in Situ Spectroscopy and High-Field Imaging. *Anal. Chem.* **2014**, *86* (3), 1767–1774.

(29) Barskiy, D. A.; Kovtunov, K. V.; Koptyug, I. V.; He, P.; Groome, K. A.; Best, Q. A.; Shi, F.; Goodson, B. M.; Shchepin, R. V.; Coffey, A. M.; et al. The Feasibility of Formation and Kinetics of NMR Signal Amplification by Reversible Exchange (SABRE) at High Magnetic Field (9.4 T). *J. Am. Chem. Soc.* **2014**, *136* (9), 3322–3325.

(30) Barskiy, D. A.; Kovtunov, K. V.; Koptyug, I. V.; He, P.; Groome, K. A.; Best, Q. A.; Shi, F.; Goodson, B. M.; Shchepin, R. V.; Truong, M. L.; et al. In Situ and Ex Situ Low-Field NMR Spectroscopy and MRI Endowed by SABRE Hyperpolarization. *ChemPhysChem* **2014**, *15* (18), 4100–4107.

(31) Knecht, S.; Pravdivtsev, A. N.; Hövener, J.-B.; Yurkovskaya, A. V.; Ivanov, K. L. Quantitative Description of the SABRE Process: Rigorous Consideration of Spin Dynamics and Chemical Exchange. *RSC Adv.* **2016**.

(32) Knecht, S.; Pravdivtsev, A. N.; Hövener, J.-B.; Yurkovskaya, A. V.; Ivanov, K. L. Quantitative Description of the SABRE Process: Rigorous Consideration of Spin Dynamics and Chemical Exchange. *RSC Adv.* **2016**, *6* (29), 24470–24477.

(33) Eshuis, N.; Hermkens, N.; van Weerdenburg, B. J. A.; Feiters, M. C.; Rutjes, F. P. J. T.; Wijmenga, S. S.; Tessari, M. Toward Nanomolar Detection by NMR Through SABRE Hyperpolarization. *J. Am. Chem. Soc.* **2014**, *136* (7), 2695–2698.

(34) Coffey, A. M.; Kovtunov, K. V.; Barskiy, D. A.; Koptyug, I. V.; Shchepin, R. V.; Waddell, K. W.; He, P.; Groome, K. A.; Best, Q. A.; Shi, F.; et al. High-Resolution Low-Field Molecular Magnetic Resonance Imaging of Hyperpolarized Liquids. *Anal. Chem.* **2014**, *86* (18), 9042–9049.

(35) Ratering, D.; Baltes, C.; Nordmeyer-Massner, J.; Marek, D.; Rudin, M. Performance of a 200-MHz Cryogenic RF Probe Designed for MRI and MRS of the Murine Brain. *Magn. Reson. Med.* **2008**, *59* (6), 1440–1447.

(36) Burns, M. J.; Rayner, P. J.; Green, G. G. R.; Highton, L. A. R.; Mewis, R. E.; Duckett, S. B. Improving the Hyperpolarization of 31P Nuclei by Synthetic Design. *J. Phys. Chem. B* **2015**, *119* (15), 5020–5027.

(37) V. Zhivonitko, V.; V. Skovpin, I.; V. Koptyug, I. Strong 31 P Nuclear Spin Hyperpolarization Produced via Reversible Chemical Interaction with Parahydrogen. *Chem. Commun.* **2015**, *51* (13), 2506–2509.

(38) Shchepin, R. V.; Barskiy, D. A.; Coffey, A. M.; Theis, T.; Shi, F.; Warren, W. S.; Goodson, B. M.; Chekmenev, E. Y. 15N Hyperpolarization of Imidazole-15N2 for Magnetic Resonance pH Sensing Via SABRE-SHEATH. *ACS Sens.* **2016**.

(39) Hennig, J.; Nauerth, A.; Friedburg, H. RARE Imaging: A Fast Imaging Method for Clinical MR. *Magn. Reson. Med.* **1986**, *3* (6), 823–833.

(40) Hövener, J.-B.; Zwick, S.; Leupold, J.; Eisenbeiβ, A.-K.; Scheifele, C.; Schellenberger, F.; Hennig, J.; Elverfeldt, D. v.; Ludwig, U. Dental MRI: Imaging of Soft and Solid Components without Ionizing Radiation. *J. Magn. Reson. Imaging* **2012**, *36* (4), 841–846.

(41) Flügge, T.; Hövener, J.-B.; Ludwig, U.; Eisenbeiss, A.-K.; Spittau, B.; Hennig, J.; Schmelzeisen, R.; Nelson, K. Magnetic Resonance Imaging of Intraoral Hard and Soft Tissues Using an Intraoral Coil and FLASH Sequences. *Eur. Radiol.* **2016**, 1–8.

(42) Ludwig, U.; Eisenbeiss, A.-K.; Scheifele, C.; Nelson, K.; Bock, M.; Hennig, J.; Flügge, T.; Hövener, J.-B. Dental MRI Using Wireless Intraoral Coils. *Sci. Rep.* **2015**, *revision*.

(43) Ohsawa, I.; Ishikawa, M.; Takahashi, K.; Watanabe, M.; Nishimaki, K.; Yamagata, K.; Katsura, K.; Katayama, Y.; Asoh, S.; Ohta, S. Hydrogen Acts as a Therapeutic Antioxidant by Selectively Reducing Cytotoxic Oxygen Radicals. *Nat. Med.* **2007**, *13* (6), 688–694.

(44) Dole, M.; Wilson, F. R.; Fife, W. P. Hyperbaric Hydrogen Therapy: A Possible Treatment for Cancer. *Science* **1975**, *190* (4210), 152–154.

(45) Coffey, A. M.; Truong, M. L.; Chekmenev, E. Y. Low-Field MRI Can Be More Sensitive than High-Field MRI. *J. Magn. Reson.* **2013**, *237*, 169–174.

(46) Inglis, B.; Buckenmaier, K.; SanGiorgio, P.; Pedersen, A. F.; Nichols, M. A.; Clarke, J. MRI of the human brain at 130 microtesla http://www.pnas.org (accessed Mar 8, 2016).

(47) Liu, G.; Song, X.; Chan, K. W. Y.; McMahon, M. T. Nuts and Bolts of Chemical Exchange Saturation Transfer MRI. *NMR Biomed.* **2013**, *26* (7), 810–828.

(48) Rose, H. M.; Witte, C.; Rossella, F.; Klippel, S.; Freund, C.; Schröder, L. Development of an Antibody-Based, Modular Biosensor for 129Xe NMR Molecular Imaging of Cells at Nanomolar Concentrations. *Proc. Natl. Acad. Sci.* **2014**, 201406797.

(49) Zotev, V. S.; Owens, T.; Matlashov, A. N.; Savukov, I. M.; Gomez, J. J.; Espy, M. A. Microtesla MRI with Dynamic Nuclear Polarization. *J. Magn. Reson.* **2010**, *207* (1), 78–88.